Hypersonic Transitional and Turbulent Flow Studies on a Lifting Entry Vehicle

C. H. YOUNG,* D. C. REDA,† AND A. M. ROBERGE*
Convair Aerospace/General Dynamics, San Diego, Calif.

An experimental and analytical program was conducted to obtain turbulent heat-transfer and boundary-layer transition data on a lifting entry configuration at Mach 10. Heat-transfer and static pressure distributions, shadowgraphs, and boundary-layer flowfield surveys were obtained. Transitional and turbulent data were taken over a range of angle of attack from $-10°$ to $60°$ and freestream unit Reynolds numbers from 300,000 to 2,400,000/ft. Transition onset, transition zone heat transfer and extent, and turbulent heat transfer were correlated with existing theories and criteria. Transition occurred at much lower Reynolds numbers on the flat lower surface than has been observed on sharp or blunt cones under similar operating conditions. No transition was observed on the conical upper surface, even at negative vehicle angles of attack.

Nomenclature

i = enthalpy (Btu/lbm)
L = model reference length (in.)
M = Mach number
$N.S.E.$ = normal shock expansion flowfield
P = pressure (lbf/in.^{2})
P_{oy} = pitot pressure (lbf/in.^{2})
q = heat-transfer rate (Btu/ft^2-sec)
r = radius (in.)
Re = Reynolds number
Re_θ = Reynolds number based on momentum thickness
t = time (sec)
T = temperature (°R)
TW = tangent wedge flowfield (oblique shock)
TW/PM = tangent wedge/Prandtl-Meyer flowfield
X = axial distance from nose
y, Y = distance normal to model surface (in.)
α = vehicle angle of attack (deg)
α_{body} = body surface inclination relative to model centerline
α_{eff} = effective angle of attack of a vehicle surface, $\alpha + \alpha_{body}$
$\alpha_{eff,l}, \alpha_{eff,u}$ = effective angle of attack of the lower and upper surface centerline
θ = boundary-layer momentum thickness
μ = viscosity (lbf-sec/ft^2)
ρ = gas density (slugs/ft^3)

Subscripts

e,E = boundary-layer edge conditions
end = end of transition zone
s = stagnation condition
TR = transition onset value
w = wall condition
x = local condition based on X
∞ = freestream condition

Superscript

$*$ = reference condition (Eckert)

Introduction

ACCURATE assessment of the aerothermodynamic environment imposed during atmospheric entry is of importance to developing reusable space transportation systems. Of critical concern are the related problems of boundary-layer transition and heat transfer in the transitional and turbulent flow regions. Numerous analytical and experimental studies have yielded solutions for elementary shapes at low angles of attack, but data at higher angles of attack, and for more complex geometries typical of actual vehicle configurations, are still lacking.

To enhance understanding of the transitional process and the resulting heat transfer on a lifting entry vehicle shape, an experimental program was conducted in Tunnel C of the AEDC von Kármán Gas Dynamics Facility. Tests were conducted at a freestream Mach number of 10 over a freestream unit Reynolds number range of 0.3–2.4 $\times$ 10^6/ft stagnation conditions from 450 to 1200 psia at 1835°R, and angles of attack from $-10°$ through 60°. The wall-to-recovery temperature ratio was approximately 0.3.

Model Descriptions

The Multipurpose Reusable Spacecraft (MRS) configuration used in the test program evolved from design studies conducted by Convair Aerospace. The basic geometry of the vehicle was developed to provide a maximum lift-to-drag ratio of 2.0 at hypersonic speeds. Figure 1 illustrates the configuration selected for this study. The lower or lifting surface was composed of two planar areas: 1) a front ramp, immediately downstream of the blunt nose region, delta in planform, and inclined at an angle of 6.75° to the vehicle centerline and 2) an aft ramp, rectangular in planform, and oriented parallel to the vehicle centerline. The angular change or "break" occurred at an X/L station of 0.4. A 15° half-angle cone formed the forward portion of the upper surface.

The thin-skin stainless-steel model of this configuration was 2.155 ft long, and instrumented with 98 iron-constantan thermocouples. For pressure tests and boundary-layer and flowfield surveys, a thick-wall stainless-steel model was used. Ninety-nine pressure tubes and eight thermocouple leads were passed through the model sting support system.

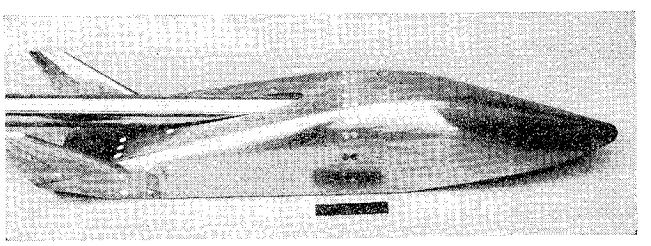

Fig. 1 Heat-transfer model.

Presented as Paper 71-100 at the AIAA 9th Aerospace Sciences Meeting, New York, January 25–27, 1971; submitted March 15, 1971; revision received July 28, 1972.

Index categories: Boundary Layers and Convective Heat Transfer —Turbulent; Re-Entry Vehicle Testing.

* Senior Thermodynamics Engineer.

† Senior Thermodynamics Engineer; presently NRC Post-Doctoral Research Associate, NASA Ames Research Center, on leave of absence from Convair Aerospace. Member AIAA.

Test Description

Heat-transfer data were obtained from the instrumented thin-skin model by the transient temperature technique. This technique consists of injecting a cool model into the tunnel air stream at the desired attitude and recording on magnetic tape the rise in model surface temperature with time. Injection time was approximately 1 sec, and the model remained at the tunnel centerline for approximately 3 sec before retraction.

On each run, temperature data T_w(°R) and dT_w/dt(°R/sec) were obtained from the center of a least-squares parabola through 21 consecutive wall temperature points at times of 0.0, 0.5, and 1.0 sec. Data were reduced to standard coefficient form using the AEDC Tunnel C general heat-transfer computer program.

Pressure tests were conducted by injecting the model into the tunnel and leaving it there until the pressure signals reached their steady-state values. Readout equipment compared successive readings of a particular tap to ensure that stabilized pressures were reached before recording data. (The Tunnel C pressure monitoring system is described in detail in Ref. 1.)

The pressure model was also used for the boundary layer and flowfield surveys at 0° and 15° angles of attack. The boundary-layer probe, furnished by AEDC, was mounted from the ceiling of the tunnel and positioned adjacent to the model with the aid of sightings taken through a transit. References 2, 3, and 4 contain detailed descriptions of all tests.

Analytic Techniques

Analytic heat-transfer computations were performed using existing computer programs described in Refs. 5–7. Two-dimensional and conical laminar heat-transfer rates at moderate angles of attack were computed using the Eckert reference enthalpy method,[8] coupled with Colburn's form of the Reynolds analogy. Laminar swept cylinder heating was calculated through a transformation of the Kemp-Riddell[9] spherical heating expression. A correction was applied to these heating rates to account for geometry effects on the stagnation line velocity gradient.[10]

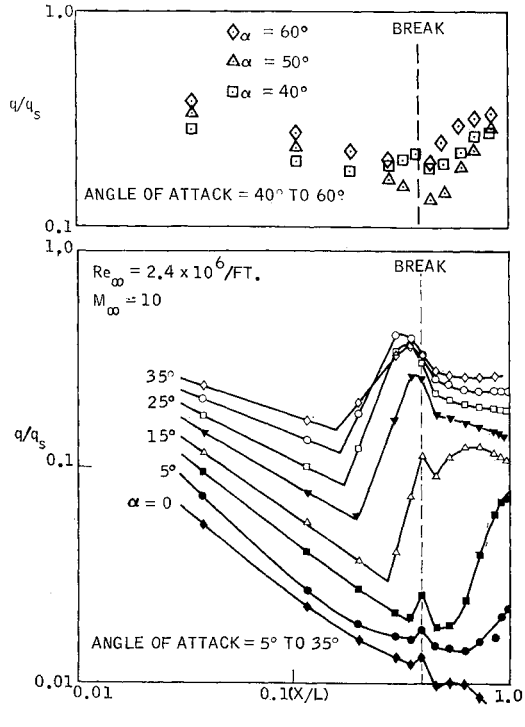

Fig. 2 Centerline heating variations with angle of attack.

Turbulent heat transfer at moderate angles of attack has been shown to correlate best using the Spalding-Chi[11] skin friction technique with the von Kármán statement of Reynolds analogy.[12] Equations used in this analysis stem from curve fits to the Spalding-Chi values developed by Komar.[13]

High angle-of-attack centerline turbulent heat-transfer rate calculations were made with the turbulent swept cylinder theory of Beckwith and Gallagher.[14] As in the laminar case, a geometry correction factor was applied to account for variation in stagnation line velocity gradient.[10]

Two methods of evaluating flowfield properties were employed in this study. The first involves curve fits of the oblique shock relations for air considered as a real gas. In conjunction with the oblique shock solution, Prandtl-Meyer expansion was used to account for changes in local body angle.

The second flowfield evaluation was the high-entropy shock layer solution. (High-entropy shock layer refers to those portions of the boundary layer and inviscid flowfield that pass through the strong blunt body or normal shock-wave region.) Stagnation properties P_s and i_s yielded a corresponding entropy value, as determined from a Mollier chart subroutine; air properties were curve-fitted as functions of pressure and entropy. Values for entropy and local static pressure then defined local shock-layer conditions, assuming an isentropic expansion from the stagnation conditions to the local pressure. Both measured and Newtonian local pressures were used but showed no appreciable difference in heat transfer. Velocity divided by computed local speed of sound gave the Mach number needed for application of the Spalding-Chi heating technique.

Heat-Transfer Correlations

Effects of angle of attack and freestream unit Reynolds number on the lower surface centerline heat-transfer distribution are shown in Figs. 2 and 3. Figure 2 illustrates the fundamental difference between heat-transfer behavior at low angle of attack (0°–35°) and high angle of attack (40°–60°). Laminar and turbulent heating rates increased with increasing angle of attack up to 35°. At 40° angle of attack and above (at an effective front ramp angle of attack of 46.75° and above), the heating rates leveled off on the back ramp. These rates appear to be turbulent, but the data are not conclusive. Lower surface shock-wave standoff distances were observed to increase at the high angles of attack, and computed flowfield properties indicated subsonic flow. Figure 3 shows heat-transfer variations with freestream unit Reynolds number at low and high angles of attack.

A further indication of the differing character of high and low angle-of-attack flowfields was obtained through comparison with existing heat-transfer theories (Fig. 4). At low angles of attack, front ramp laminar heat-transfer levels correlated with predictions of the Eckert reference enthalpy

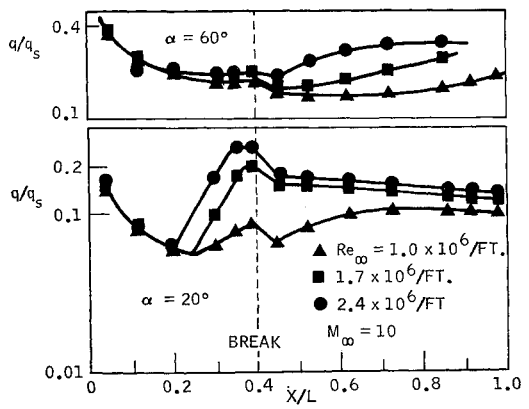

Fig. 3 Centerline heating variations with Re_∞.

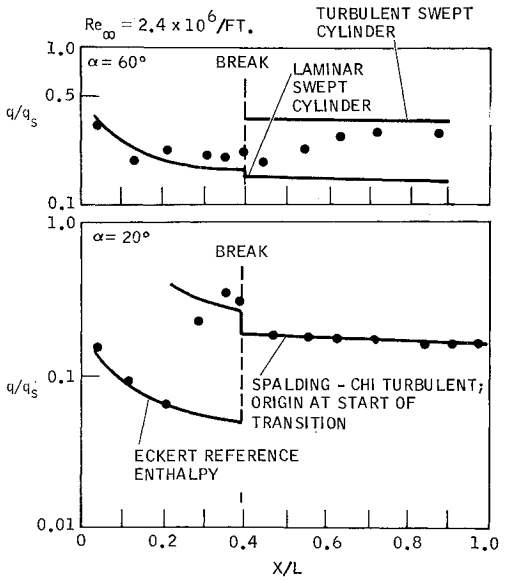

Fig. 4 Heat-transfer correlation.

technique,[8] coupled with a normal shock-expansion (high entropy) flowfield. Back ramp turbulent data correlated with predictions of the Spalding-Chi theory,[11] coupled with a tangent wedge/Prandtl-Meyer (low entropy) flowfield. Justification for the change in flowfield assumptions is discussed below.

High angle-of-attack flowfields were more closely approximated by swept cylinder theory. Both laminar[7] and turbulent[14] swept cylinder theories, corrected for stagnation line velocity gradient effects,[10] gave good agreement with the data.

Figure 5 presents upper surface centerline heating distributions for vehicle angles of attack from $-10°$ to $0°$. Since the upper surface is essentially a 15° half-angle cone, this represents surface inclination angles of 25°–15° relative to the freestream. At higher Reynolds numbers, no negative angles of attack were run. Laminar heat-transfer predictions are seen

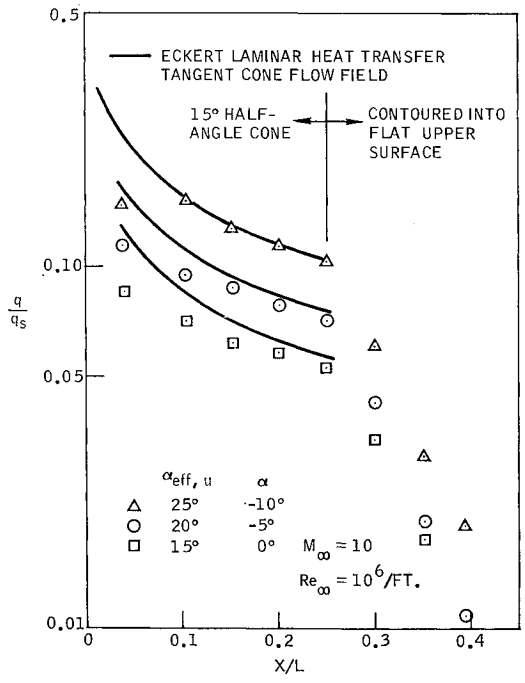

Fig. 5 Upper surface centerline heat-transfer distributions.

to correlate well with the data using a conical oblique shock flowfield. No transition or turbulence was observed on the conical upper surface.

Transition Onset

Transition onset locations for the combined angle-of-attack freestream unit Reynolds number range tested are summarized in Fig. 6, and were determined from log-log plots of the lower surface centerline heat-transfer distributions; e.g., Fig. 2. Use of transition location as a parameter of interest was indicated by an invariance with Reynolds number from 10° to 30°.

Transition first appeared on the aft ramp and progressed forward to the front ramp with increasing angle of attack. Transition onset location $(X/L)_{TR}$ was relatively insensitive to freestream unit Reynolds number over the angle-of-attack range of 10°–30°. A sudden rearward shift in these trends occurred between 30° and 40° angle of attack (i.e., at effective front ramp angles of attack between 36.75° and 46.75°). A second forward progression of transition onset with increasing angle of attack occurred for $\alpha \geq 50°$.

Upon closer examination of the available pitot pressure surveys (Figs. 7 and 8) and shadowgraph pictures, an important feature of the low angle-of-attack flow ($\alpha \leq 30°$) was revealed, and a possible mechanism for the observed transition behavior suggested. A sequence of shadowgraphs, taken over the angle-of-attack range of 10°–20°, is shown in Fig. 9. Shock shapes exhibit an inflection point similar to flows known to occur about blunted cones at angles of attack.[15,16] This inflection point presents a minimum shock angle relative to the freestream flow. Through this minimum shock angle passes a line of maximum total pressure and maximum unit Reynolds number, i.e., the line that separates the high-entropy (blunt nose) vortical flow region from the low entropy or oblique shock flowfield. Flowfield surveys such as shown in Fig. 7 reveal the location of this peak total pressure line. Also emanating from each inflection point in Fig. 9 is a white line which is the maximum rate of change of density gradient $(\partial^2\rho/\partial y^2)$. The location at which the white line begins to interact with the boundary layer appears just ahead of the point at which boundary-layer transition was indicated by heat-transfer measurements (arrows in Fig. 9). By extrapolating the white line until it intersects the lower surface, a good indication of the transition location was obtained. The range of locations for these extrapolated intersections is shown in Fig. 6. Thus it appears that as soon as the low-entropy inviscid region (outside the white line) interacts with the boundary-layer edge, transition occurs. Ahead of transition, the boundary-layer edge properties are those of a high entropy blunt body flow, while at the transition point and downstream, the boundary-layer edge is in a low entropy flow.

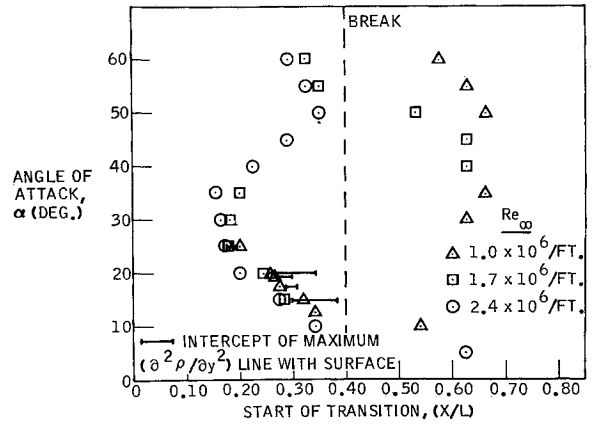

Fig. 6. Transition onset locations vs angle of attack.

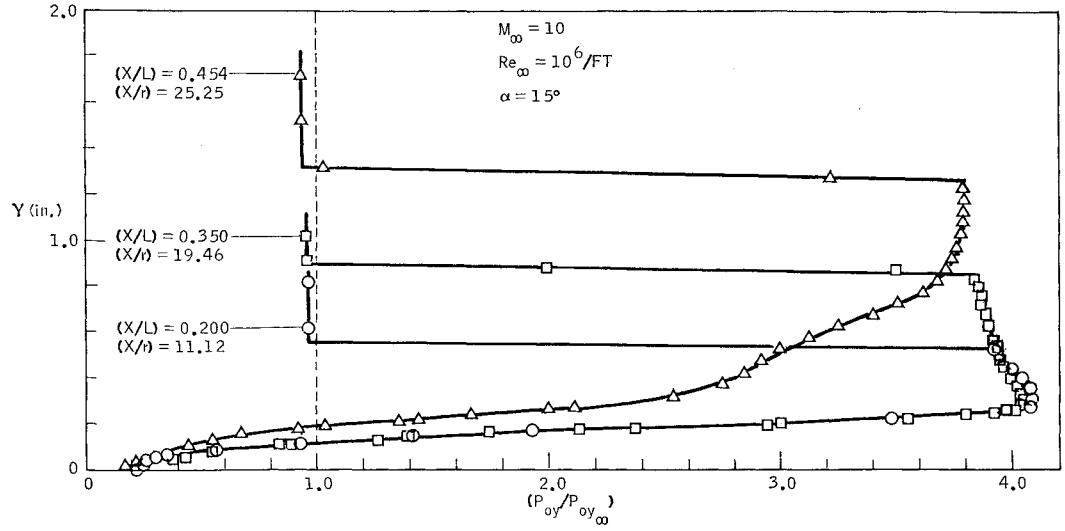

Fig. 7 Shock layer pitot pressure surveys; $\alpha = 15°$, $Re\infty = 10^6$/ft.

Pitot pressure surveys showed remarkable agreement with those measured by Cleary[15,16] in his investigations of blunt cone flowfields. When these pitot pressure surveys were superimposed on the shadowgraph pictures (Fig. 8), it became evident that the line of maximum ($\partial^2\rho/\partial y^2$) occurred between the wall and the streamline of maximum total pressure.

Existence of the strong $\partial^2\rho/\partial y^2$ gradient in the lower surface flowfield and its apparent coupling with transition onset prompted an analysis of upper surface flowfield and heat-transfer data. At zero and negative vehicle angles of attack—i.e., at effective angles of attack of $-15°$ and greater—the conical upper surface of the model yielded a more strictly axisymmetric flowfield at an equivalent blunt nose radius.

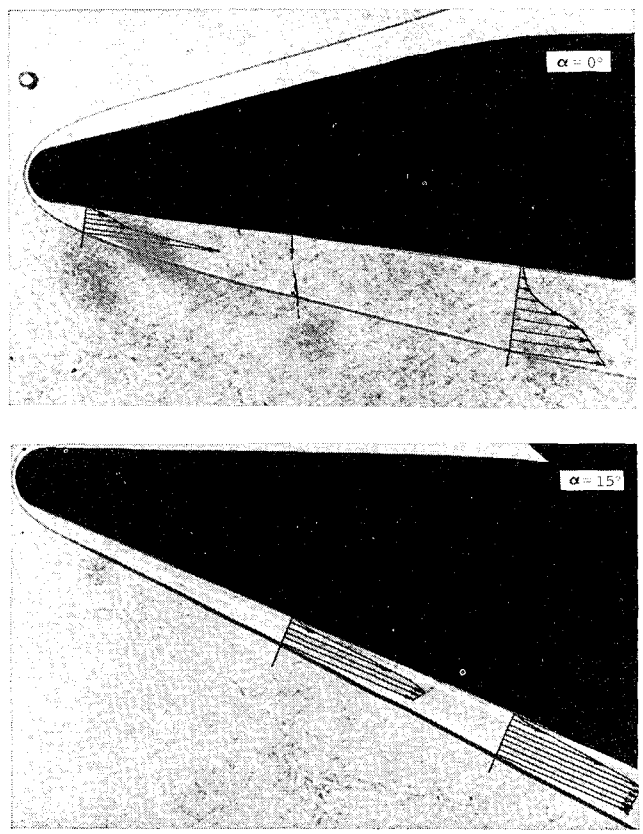

Fig. 8 Pitot pressure surveys superimposed on shadowgraphs; $Re\infty = 10^6$/ft.

Comparisons between lower and upper surface flowfield shadowgraphs taken at equivalent effective angles of attack showed significant differences. Shock-wave inflection points on the upper surface were located further aft, and the strong $\partial^2\rho/\partial y^2$ gradient was not present in the upper surface pictures. Further, no boundary-layer transition was observed on the upper surface over the entire angle of attack/freestream unit Reynolds number range tested.

The geometry of the lower surface, consisting of a blunt nose fairing immediately into a flat surface, promotes a complex three-dimensional flowfield as the blunt nose flow region expands to accommodate the planar surface. This accommodation of the lower surface flowfield forces the shock-wave inflection point forward from the location that it would assume in a strictly axisymmetric flow and generates more severe gradients in the various flowfield thermodynamic properties. Transition onset then occurs as a result of the interaction between this complex three-dimensional inviscid flowfield and the boundary layer that must develop within it.

On the upper surface for all angles, and on the lower surface at small vehicle angles of attack where such strong interactions between the inviscid flow and the boundary layer did not occur, it was not possible to induce transition onset, even with the aid of spherical-trip elements.

Correlation of transition onset Reynolds number as a function of unit Reynolds number and Mach number at the boundary-layer edge is presented in Fig. 10. Increases in transition Reynolds number with increasing boundary-layer edge unit Reynolds number and Mach number have been observed by other investigators (e.g., Ref. 17).

High angle-of-attack transition Reynolds numbers were also computed from the 2.4×10^6/ft data through use of the normal shock expansion flowfield technique. This technique was applied for effective body angles of attack $\alpha_{eff} \geq 46.75°$ using run lengths from the geometric stagnation point. No cross-flow corrections were applied. Low and high angle-of-attack results are combined in Fig. 11. Momentum thickness Reynolds numbers were computed by a compressible approximation suggested in Ref. 18.

Transition Zone Extent

Transition zone extent is best described by the ratio of transition end-to-onset boundary-layer edge Reynolds number (Re_{end}/Re_{TZ}). Values near 2.0 were found (Fig. 12); the ratio decreased slightly with increasing transition onset Reynolds number.

Freestream unit Reynolds number appeared to influence the length of the transition zone significantly. An examination

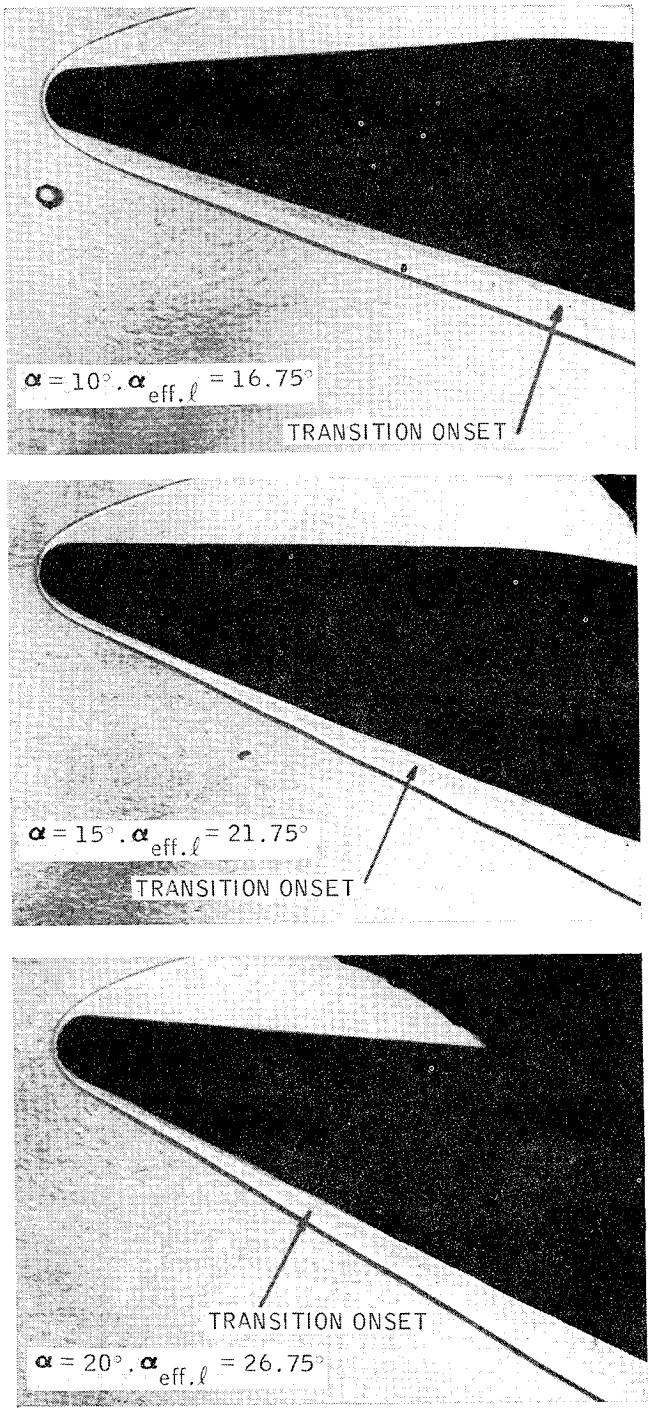

Fig. 9 Sequence of shadowgraphs over 10° to 20° angle of attack range.

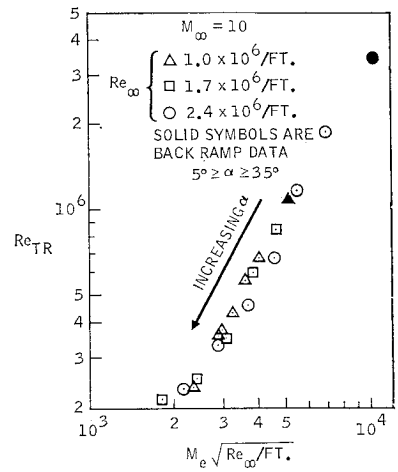

Fig. 10 Transition Reynolds number vs $M_E(Re\infty/\text{ft})^{1/2}$.

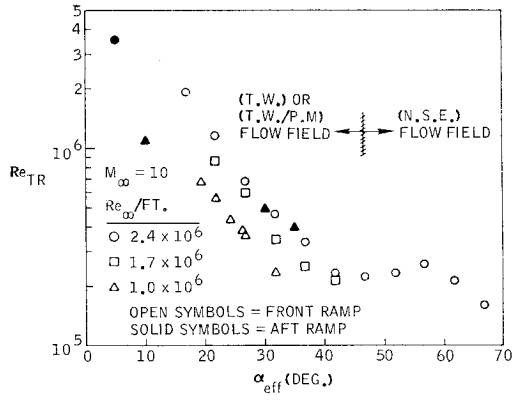

Fig. 11 Transition Reynolds number vs effective angle of attack.

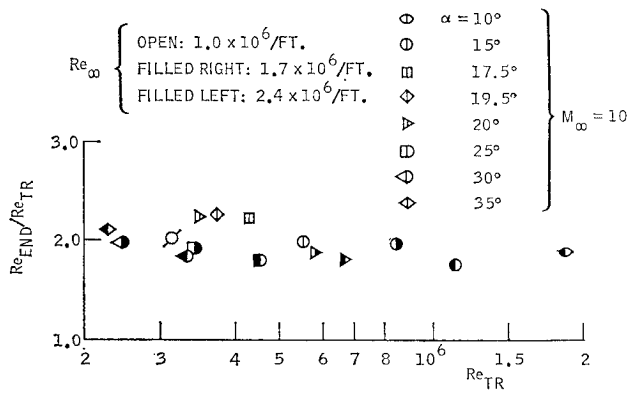

Fig. 12 Transition zone factor vs transition Reynolds number.

of Fig. 12 shows a decrease in transition zone extent with increasing freestream unit Reynolds number. For example, at 20° angle of attack, the transition zone length ratio was approximately 2.2 for a freestream unit Reynolds number of 10^6/ft, 1.85 at 1.7×10^6/ft, and 1.75 at 2.4×10^6/ft. Similar behavior was observed at other angles of attack.

Conclusions

Several significant conclusions were obtained from analysis and correlation of the AEDC wind-tunnel data taken with the MRS lifting-entry configuration.

1) Turbulent heat-transfer levels were experienced on the lower surface centerline over the 10°–35° angle-of-attack range for the highest freestream unit Reynolds number tested (2.4×10^6/ft). From 40° to 60°, the heat-transfer levels were transitional. At a unit Reynolds number of 1.0×10^6/ft, turbulent heating was obtained over an angle-of-attack range of 15°–25° on the lower surface centerline. No transitional or turbulent flow was observed on the upper surface at any angle of attack or Reynolds number tested. No lower surface transition could be detected at angles of attack of 0° and below. Attempts to trip the boundary layer artificially on the upper surface and on the lower surface at 0° angle of attack were unsuccessful.

2) Heat-transfer distributions in both the low and high

angle-of-attack regimes have been correlated with existing theories. Beckwith-Gallagher turbulent swept cylinder theory with a stagnation line velocity gradient correction showed good agreement with turbulent heat-transfer levels over the angle-of-attack range 35°–60°. Front ramp turbulent levels were best predicted by Spalding-Chi theory when used with a tangent wedge flowfield and transition point boundary-layer run lengths for the data shown. Spalding-Chi predictions, generated through use of tangent wedge/Prandtl-Meyer flowfields and transition point boundary-layer run lengths, consistently bounded the aft ramp turbulent data.

3) Transition onset location was found to be a strong function of vehicle geometry and angle of attack—great caution should be exercised in extrapolating low angle-of-attack transition results to higher angles of attack. The complex blunt nose inviscid flowfield on the forward portion of the vehicle lower surface has been identified as a major contributor to transition onset over the angle-of-attack range 10°–30°. Present transition Reynolds number values were found to correlate with the parameter $M_E(Re\infty/\text{ft})^{1/2}$ for angles of attack from 5° to 35°. Finite transition zones were observed throughout the angle-of-attack range tested. Transition zone lengths were found to be approximately equal to transition onset lengths, i.e., $Re_{\text{end}}/Re_{TR} \cong 2.0$. Transition zone extent decreased with increasing freestream unit Reynolds number.

References

[1] *Test Facilities Handbook*, 7th ed., Arnold Engineering Development Center, Arnold Air Force Station, Tenn., 1968.

[2] Carman, J. B., Jr. and Strong, M. G., "Aerothermodynamic Characteristics of a Multipurpose Entry Vehicle at Mach Number 10," AEDC-TR-68-276, Feb. 1969, Arnold Engineering Development Center, Arnold Air Force Station, Tenn.

[3] Spurlin, C. J., "Heat Transfer Tests of a Multipurpose Entry Vehicle at Mach Number 10," AEDC-TR-69-206, Feb. 1969, Arnold Engineering Development Center, Arnold Air Force Station, Tenn.

[4] Spurlin, C. J. and Edmunds, E. W., "Heat Transfer Tests of a Multipurpose Reusable Spacecraft (MRS) at Mach Number 10," AEDC-TR-70-132, June 1970, Arnold Engineering Development Center, Arnold Air Force Station, Tenn.

[5] Whitehead, K. D., "Computer Program 3020 Revision," Rept. GDC-ERR-1416, Dec. 1969, Convair Aerospace/General Dynamics Corp., San Diego, Calif.

[6] Scullen, R. S., "A Description of the Revised Aerodynamic/Structural Heating and Radiation Equilibrium Temperature Computer Program 3020," Rept. GDC-ERR-1336, Dec. 1968, Convair Aerospace/General Dynamics Corp., San Diego, Calif.

[7] Young, C. H., Reda, D. C., and Roberge, A. M., "Hypersonic Flow Field and Heat Transfer Studies on a Lifting Entry Vehicle at Angles of Attack from 0° to 60°," Rept. GDC-ERR-1418, Sept. 1970, Convair Aerospace/General Dynamics Corp., San Diego, Calif.

[8] Eckert, E. R., "Survey of Heat Transfer at High Speeds," WADC TR 54-70, 1954, Wright Air Development Center, Dayton, Ohio.

[9] Kemp, N. H. and Riddell, F. R., "Heat Transfer to Satellite Vehicles Re-Entering the Atmosphere," *Jet Propulsion*, Vol. 27, No. 2, Feb. 1957, pp. 132–137, 147.

[10] Bertram, M. H., Feller, W. V., and Dunavant, J. C., "Flow Fields, Pressure Distributions, and Heat Transfer for Delta Wings at Hypersonic Speeds," TM-X-316, Sept. 1960, NASA.

[11] Spalding, D. B. and Chi, S. W., "The Drag of a Compressible Turbulent Boundary Layer on a Smooth Flat Plate With and Without Heat Transfer," *Journal of Fluid Mechanics*, Vol. 18, Pt. I, Jan. 1964, pp. 117–143.

[12] Young, C. H., Roberge, A. M., and Reda, D. C., "Aerodynamic Analyses of a Lifting Entry Vehicle at Mach 10," Rept. GDC-ERR-1415, March 1970, Convair Aerospace/General Dynamics Corp., San Diego, Calif.

[13] Komar, J. J., "Improved Turbulent Skin-Friction Coefficient Predictions Utilizing the Spalding-Chi Method," DAC-59801, Nov. 1966, Douglas Aircraft Co., Santa Monica, Calif.

[14] Beckwith, I. E. and Gallagher, J. J., "Local Heat Transfer and Recovery Temperatures on a Yawed Cylinder at a Mach Number of 4.15 and High Reynolds Numbers," TR-R-104, 1961, NASA.

[15] Cleary, J. W., "Effects of Angle of Attack and Nose Bluntness on the Hypersonic Flow Over Cones," AIAA Paper 66-414, Los Angeles, Calif., 1966.

[16] Cleary, J. W., "An Experimental and Theoretical Investigation of the Pressure Distribution and Flow Fields of Blunted Cones at Hypersonic Mach Numbers," TN D-2969, Aug. 1965, NASA.

[17] Hopkins, E. J. and Keener, E. R., "Unit Reynolds Number Effects on Boundary-Layer Transition at Mach 6," *AIAA Journal*, Vol. 6, No. 5, May 1968, p. 956.

[18] Freeman, G. N., "Effects of Crossrange on STS Orbiter Thermal Protection Requirements," TOR-0059 (6758-02)-2, 1970, The Aerospace Corp., El Segundo, Calif.